Geophysical Research Letters

RESEARCH LETTER
10.1029/2020GL089189

Unsteady Ekman-Stokes Dynamics: Implications for Surface Wave-Induced Drift of Floating Marine Litter

C. Higgins[1,2], J. Vanneste[2], and T. S. van den Bremer[1]

[1]Department of Engineering Science, University of Oxford, Oxford, UK, [2]School of Mathematics and Maxwell Institute for Mathematical Sciences, University of Edinburgh, Edinburgh, UK

Key Points:

- Marine litter studies include surface wave transport by Stokes drift but have neglected wave-induced Eulerian-mean flows in the upper ocean
- We present a model of the Eulerian-mean Ekman-Stokes response to time-varying Stokes drift for use in marine litter transport models
- Using buoy data, we show that the unsteady Ekman-Stokes flow significantly alters both magnitude and direction of near-surface transport

Supporting Information:

- Text S1
- Text S2
- Text S3
- Text S4
- Data Set S1
- Data Set S2
- Data Set S3
- Data Set S4
- Data Set S5
- Data Set S6
- Data Set S7

Correspondence to:
C. Higgins,
christopher.higgins@keble.ox.ac.uk

Citation:
Higgins, C., Vanneste, J., & van den Bremer, T. S. (2020). Unsteady Ekman-Stokes dynamics: Implications for surface wave-induced drift of floating marine litter. *Geophysical Research Letters*, *47*, e2020GL089189. https://doi.org/10.1029/2020GL089189

Received 11 JUN 2020
Accepted 27 AUG 2020
Accepted article online 2 SEP 2020

Abstract We examine Stokes drift and wave-induced transport of floating marine litter on the surface of a rotating ocean with a turbulent mixed layer. Due to Coriolis-Stokes forcing and surface wave stress, a second-order Eulerian-mean flow forms, which must be added to the Stokes drift to obtain the correct wave-induced Lagrangian velocity. We show that this wave-driven Eulerian-mean flow can be expressed as a convolution between the unsteady Stokes drift and an "Ekman-Stokes kernel." Using this convolution, we calculate the unsteady wave-driven contribution to particle transport. We report significant differences in both direction and magnitude of transport when the Eulerian-mean Ekman-Stokes velocity is included.

Plain Language Summary In transport models for floating marine litter, surface wave effects are often included by simply superimposing their Stokes drift (the small net drift induced by waves) upon wind-driven flows and currents. However, due to Earth's rotation and turbulent dissipation in the ocean's surface mixed layer, the Stokes drift also drives additional Eulerian-mean flows. To obtain the correct transport velocity, the wave-induced Eulerian-mean flow must be added to the Stokes drift. We develop a model that enables estimation of this wave-induced Eulerian-mean flow from measurements or predictions of the wave field and apply our model to buoy data. Accounting for the wave-induced Eulerian-mean flow significantly alters predictions of transport of floating marine litter by waves.

1. Introduction

Floating marine debris, including plastic pollution, has rapidly become one of the most pressing environmental problems (Eriksen et al., 2014), particularly for marine ecosystems (Lavender Law, 2017). Although consensus exists about the longevity of plastic in the marine environment (Andrady, 2011) and the relatively large buoyancy of a significant share of plastic produced (Geyer et al., 2017), with both factors contributing to their long-distance transport, the total plastic budget of the world's oceans is poorly understood. A significant mismatch exists between the estimated amount of land-generated plastic that enters coastal waters (5–12 million tonnes year^{-1} Jambeck et al., 2015) and the estimated total amount of plastic floating at sea (less than 0.3 million tonnes Cózar et al., 2014; Eriksen et al., 2014; van Sebille et al., 2015). Similarly, the amount of plastics measured at sea over the last few decades (Lebreton et al., 2019; Ostle et al., 2019; Wilcox et al., 2020) has not kept pace with growth in global plastic production (Geyer et al., 2017; Goldstein et al., 2012). To understand this mismatch, an improved understanding of the physical processes governing transport and dispersion is required (van Sebille et al., 2020). This letter focuses on one of these processes: surface waves.

As a particle undergoes its periodic motion beneath surface waves, it experiences a Lagrangian-mean velocity in the waves' direction known as Stokes drift (Stokes, 1847). More generally, Stokes drift is the difference between the average Lagrangian velocity of a fluid parcel and the average Eulerian velocity of the fluid measured at a fixed spatial location (e.g., Bühler, 2014; van den Bremer & Breivik, 2017). Surface gravity waves on the open ocean are mostly caused by winds. At any location and time, the wave field is a superposition of waves that have been generated by earlier winds at another location. Wave models, such as WAM (The WAMDI Group, 1988) and WaveWatch-III (Tolman, 2009), have been developed to predict wave fields and thus Stokes drift (Breivik et al., 2014; Webb & Fox-Kemper, 2011).

A recent and growing body of literature is examining the role of Stokes drift in the transport and dispersion of floating plastic pollution. Iwasaki et al. (2017) showed that in the Sea of Japan, Stokes drift pushed microplastics closer to the coast. Delandmeter and van Sebille (2019) and Onink et al. (2019) report a similar result in Arctic regions. Dobler et al. (2019) demonstrated that Stokes drift fundamentally changes transport patterns in the South Indian Ocean by shifting the convergence regions to the west, causing leakage into the South Atlantic rather than the South Pacific. Waves may also allow particles to cross strong circumpolar winds and currents (Fraser et al., 2018).

Crucially, the above studies have simply superimposed the Stokes drift obtained from the local wave field onto the Eulerian current field obtained from ocean general circulation models or observations. In doing so, they have ignored the fact that the Eulerian flow is itself modified by surface waves: On the rotating Earth, the Coriolis force associated with the Stokes drift drives an Eulerian-mean current in the turbulent upper-ocean boundary layer (Hasselmann, 1970; Lewis & Belcher, 2004; Ursell, 1950; Xu & Bowen, 1994), as noted in Onink et al. (2019). Together with the Stokes drift and the nonwave background flow, this wave-induced Eulerian current forms the Lagrangian velocity with which marine litter is transported. It is this wave-induced Eulerian current, which we call the Ekman-Stokes flow, that this letter examines.

We derive a model for computing the unsteady Eulerian-mean Ekman-Stokes response to a time-varying Stokes drift, taking into account the correct wave stress boundary condition and the Coriolis-Stokes forcing. We do so for the case of constant eddy viscosity in the turbulent upper-ocean layer and a quasi-monochromatic (or narrow-banded) wave field, and zero initial wave-induced Eulerian-mean velocity $\overline{\boldsymbol{u}} = \boldsymbol{0}$. The product of this letter is an Ekman-Stokes convolution kernel, which can readily be used to predict the wave-induced Eulerian-mean flow in the turbulent upper-ocean boundary layer and hence the Lagrangian transport of floating marine debris. This kernel is a low-computational-cost alternative to fully coupled general circulation and wave models, which include the effect of waves in both the Coriolis-Stokes forcing and the surface boundary condition (Breivik et al., 2015). Using sample wave field data from buoys, we show that accounting for the Eulerian-mean Ekman-Stokes response to a time-varying Stokes drift considerably alters the trajectories of drifting objects.

2. Unsteady Ekman-Stokes Flow

We consider a homogeneous (constant-density), incompressible ocean of constant depth d, described by horizontal coordinates x and y and a vertical coordinate z measured upward from the undisturbed water level. The governing equations, divided through by the (constant) density ρ, are

$$\partial_t \boldsymbol{u} + \boldsymbol{u}\cdot\boldsymbol{\nabla}\boldsymbol{u} + \boldsymbol{f}\times\boldsymbol{u} = -\boldsymbol{\nabla}p + \nu\nabla^2\boldsymbol{u}, \qquad \boldsymbol{\nabla}\cdot\boldsymbol{u} = 0, \tag{1a}$$

$$w|_{z=\eta} = \partial_t\eta + \boldsymbol{u}_{\mathrm{H}}|_{z=\eta}\cdot\boldsymbol{\nabla}_{\mathrm{H}}\eta, \qquad \hat{\boldsymbol{n}}\cdot\overleftrightarrow{\boldsymbol{\tau}}\cdot\hat{\boldsymbol{s}}|_{z=\eta} = 0, \tag{1b}$$

$$w|_{z=-d} = 0, \tag{1c}$$

where $z=\eta(x,y,t)$ denotes the free surface elevation, $\boldsymbol{u}$ is the three-dimensional velocity vector, $\boldsymbol{f}$ the Coriolis vector, $\boldsymbol{A}_{\mathrm{H}} \equiv \left(A_x, A_y, 0\right)$ the horizontal component of any $\boldsymbol{A}$, and $\overleftrightarrow{\boldsymbol{\tau}}$ the stress tensor with components $\tau_{ij} = -(p-p_0)\delta_{ij} + \nu(\partial_i u_j + \partial_j u_i)$, with p_0 the atmospheric pressure divided by the (constant) density ρ and ν the turbulent eddy viscosity, taken constant. The unit vectors $\hat{\boldsymbol{n}}$ and $\hat{\boldsymbol{s}}$ are normal and tangential to the free surface respectively, so (1b) is a stress-free condition.

2.1. Wave-Averaged Mean-Flow Equations

We assume the wave steepness is small, $\alpha \equiv kA \ll 1$, where A is the peak wave amplitude of η and k the peak wave number, and solve (1) to $O(\alpha^2)$ using a Stokes expansion $\boldsymbol{u} = \boldsymbol{u}_1 + \boldsymbol{u}_2 + \ldots$, where the subscript denotes the order in α. We focus on deep water waves ($kd \gg 1$).

Linear wave dynamics arises at $O(\alpha)$, where we ignore viscous effects, neglecting a thin vorticity boundary layer of thickness $\delta_\nu = \sqrt{2\nu/\omega}$ under the (generally satisfied) assumption $k\delta_\nu \ll 1$. Consequently, we ignore viscous damping of waves as they propagate. In contrast, the Coriolis force must be retained since, as demonstrated by Hasselmann (1970), $O(f/\omega)$ corrections put horizontal and vertical velocity components out of quadrature, with impact on the wave-averaged dynamics.

Integrating the $O(\alpha^2)$ equations over a wave period, we obtain the wave-averaged mean flow equations (e.g., Huang, 1979; Suzuki & Fox-Kemper, 2016)

$$\partial_t \overline{u} - f v_{\mathrm{L}} = -\partial_x \overline{p} + \nu \nabla^2 \overline{u}, \qquad \partial_t \overline{v} + f u_{\mathrm{L}} = -\partial_y \overline{p} + \nu \nabla^2 \overline{v}, \tag{2a}$$

$$\partial_t \overline{w} = -\partial_z \overline{p} + \nu \nabla^2 \overline{w}, \qquad \partial_x \overline{u} + \partial_y \overline{v} = -\partial_z \overline{w}, \tag{2b}$$

where the overbar denotes a time average; $\boldsymbol{u}_{\mathrm{L}} = \overline{\boldsymbol{u}} + \boldsymbol{u}_{\mathrm{S}}$ is the Lagrangian (or particle transport) velocity associated with the waves, with $\overline{\boldsymbol{u}} = \overline{\boldsymbol{u}_2}$ the wave-induced Eulerian-mean velocity and $\boldsymbol{u}_{\mathrm{S}}$ the Stokes drift; and the horizontal component of the Coriolis vector introduces only higher-order corrections to the flow. To derive (2a) and (2b), we assumed that the nonwave background flow has small Rossby number, $|\boldsymbol{\nabla}\times\boldsymbol{u}_{\mathrm{B}}|/f \ll 1$. It follows that the corresponding Stokes vortex force $\left(\boldsymbol{\nabla}\times\boldsymbol{u}_{\mathrm{B}}\right)\times\boldsymbol{u}_{\mathrm{S}}$ is negligible compared with the Coriolis-Stokes term, while $\left(\boldsymbol{\nabla}\times\overline{\boldsymbol{u}}\right)\times\boldsymbol{u}_{\mathrm{S}}$ is $O(\alpha^4)$ since it involves only the wave-induced flow (Suzuki & Fox-Kemper, 2016). The background $\boldsymbol{u}_{\mathrm{B}}$ can then simply be superimposed on the wave-induced Lagrangian flow $\boldsymbol{u}_{\mathrm{L}}$. Where the condition $|\boldsymbol{\nabla}\times\boldsymbol{u}_{\mathrm{B}}|/f \ll 1$ does not hold—for example, in a submesoscale front—a more complete treatment of the governing equations is required (e.g., McWilliams & Fox-Kemper, 2013).

Without the shear and pressure terms, Equations 2a and 2b correspond to those considered by Hasselmann (1970). The equations include the Coriolis-Stokes forcing $-f\hat{\boldsymbol{z}}\times\boldsymbol{u}_{\mathrm{S}}$ (Hasselmann, 1970; Polton et al., 2005), which drives an Eulerian "anti-Stokes flow," canceling the Stokes drift and exciting inertial oscillations, and explains Ursell (1950)'s prediction of zero net drift for periodic waves in a rotating frame.

We focus on the horizontal momentum Equations 2a in the Stokes layer, that is, the top $O(k^{-1})$ deep layer of the ocean where the Stokes drift and hence the Coriolis-Stokes forcing are localized. One of the boundary conditions is provided by averaging the condition of zero tangential stress in (1b) (Longuet-Higgins, 1953; Seshasayanan & Gallet, 2019; Ünlüata & Mei, 1970; Xu & Bowen, 1994); it is given by

$$\partial_z \overline{\boldsymbol{u}}_{\mathrm{H}}|_{z=0} = \partial_z \boldsymbol{u}_{\mathrm{SH}}|_{z=0}. \tag{3}$$

Examining the viscous but nonrotating case, Longuet-Higgins (1953) showed that vorticity is transported from the viscous boundary layers into the fluid interior, affecting the mass transport profile (Seshasayanan & Gallet, 2019; Ünlüata & Mei, 1970; Xu & Bowen, 1994). Within these boundary layers the flow is not irrotational, resulting in a viscous stress upon the Eulerian-mean flow. Upon expanding the second equation in (2b) about $z = 0$, performing a momentum budget, and averaging over a wave period, this leads to condition (3). Additional Eulerian-mean wave-induced transport, known as boundary-layer streaming, occurs in the boundary layer (e.g., Grue & Kolaas, 2017). The contributions of Hasselmann (1970) and Longuet-Higgins (1953) (and the theory of wind-driven currents of Ekman, 1905) were unified by Xu and Bowen (1994) into a model of wave-driven (and wind-driven) flow in finite-depth water.

In the Stokes layer, vertical gradients dominate over horizontal ones. It follows from (2b) that the vertical velocity component and pressure gradient can be neglected. Introducing the complex notation $\mathcal{U} = \overline{u} + i\overline{v}$ as in Huang (1979), we obtain the Ekman-Stokes equations

$$(\partial_t + if - \nu\partial_z^2)\mathcal{U} = -if\mathcal{U}_{\mathrm{S}}(\boldsymbol{x}, z, t), \tag{4a}$$

$$\partial_z \mathcal{U} = \partial_z \mathcal{U}_{\mathrm{S}}(\boldsymbol{x}, z, t)\big|_{z=0}, \tag{4b}$$

$$\lim_{z\to-\infty} \mathcal{U} = 0, \tag{4c}$$

where the boundary conditions follow from (3) and the requirement that the solution be matched to a weak Eulerian flow outside the Stokes layer. The Eulerian Ekman-Stokes velocity solving (4) is driven by the Stokes drift in two ways, via the Coriolis-Stokes forcing in the fluid interior (Polton et al., 2005) and via the wave stress (4b).

Note that a wind stress could be added to (4b); by linearity, the wind-driven Ekman velocity would be superimposed in convolution form on the wave-driven velocity we obtain (e.g., Madsen, 1978, Equation 21 for linearly-varying $\nu(z)$). In a coupled oceanic-atmospheric model, Lewis and Belcher (2004) derive steady solutions to (4) for nonconstant viscosity, though they do not seem to include the wave stress.

2.2. Solution by Laplace Transform

We solve (4) by Laplace transform, assuming that the Stokes drift $\mathcal{U}_S$ has a time-independent vertical structure $\exp(2kz)$ corresponding to a quasi-monochromatic wave field, but an otherwise arbitrary time dependence. Denoting the Laplace transform by a tilde, with

$$\tilde{g}(s) = \mathcal{L}\{g(t)\} = \int_0^\infty g(t)e^{-st}dt, \tag{5a}$$

$$g(t) = \mathcal{L}^{-1}\{\tilde{g}(s)\} = \frac{1}{2\pi i}\int_{\gamma-i\infty}^{\gamma+i\infty} \tilde{g}(s)e^{st}ds, \tag{5b}$$

where γ is a real number such that the contour path of integration is in the region of convergence of $\tilde{g}(s)$, we find that when $\mathcal{U}(t=0)=0$,

$$\tilde{\mathcal{U}} = 2k\left(1+\frac{if}{s+if-4k^2\nu}\right)\frac{\tilde{\mathcal{U}}_S e^{z\sqrt{(s+if)/\nu}}}{\sqrt{(s+if)/\nu}} - \frac{if\tilde{\mathcal{U}}_S e^{2kz}}{s+if-4k^2\nu}. \tag{6}$$

This is the sum of a particular solution—the second term—which can be interpreted as a partial anti-Stokes flow varying over the Stokes depth $\delta_S = (2k)^{-1}$, and a homogeneous solution—the first term—varying over the Ekman depth $\delta_E = \sqrt{2\nu/f}$, which includes a contribution driven by the vertical shear of the anti-Stokes flow through boundary condition (4b) (second term in the brackets in (6)).

A special case of (6) occurs if $\mathcal{U}_S$ approaches a steady value $\overline{\mathcal{U}_S}$ as $t\to\infty$. Then $\tilde{\mathcal{U}}$ tends to the time-independent solution (cf. Seshasayanan & Gallet, 2019)

$$\overline{\mathcal{U}} = \frac{(1-i)D}{2}\overline{\mathcal{U}_S}\left(1+\frac{1}{1+iD^2/2}\right)e^{(1+i)z/\delta_E} - \frac{\overline{\mathcal{U}_S}e^{2kz}}{1+iD^2/2}, \tag{7}$$

where $D \equiv \delta_E/\delta_S$ is the fixed ratio of Ekman to Stokes depths. In the limit $D\to 0^+$, Equation 7 approaches $-\overline{\mathcal{U}_S}\exp(2kz)$: Up to an inertial oscillation this is the so-called "anti-Stokes" Eulerian-mean flow, predicted by Hasselmann (1970) to be induced by periodic waves in a rotating, inviscid ocean. Viscosity acts to reduce the shear in the anti-Stokes flow, so that a nonzero Lagrangian-mean velocity remains.

2.3. Ekman-Stokes kernel

We now use the Laplace convolution theorem to write the unsteady solution for the Ekman-Stokes mean flow as a function of time for arbitrary Stokes drift as

$$\mathcal{U}(\boldsymbol{x}, z, t) = \mathcal{U}_S|_{z=0} * K(z,t), \tag{8}$$

where $*$ denotes convolution in time and

$$K(z,t) = \mathcal{L}^{-1}\left\{\frac{2ke^{z\sqrt{(s+if)/\nu}}}{\sqrt{(s+if)/\nu}} + \frac{if}{s+if-4k^2\nu}\left(\frac{2ke^{z\sqrt{(s+if)/\nu}}}{\sqrt{(s+if)/\nu}} - e^{2kz}\right)\right\}. \tag{9}$$

The convolution kernel $K(z,t)$, which we will term the Ekman-Stokes kernel, can be evaluated by deforming the integration contour involved in the inverse Laplace transform to obtain (see the supporting information)

$$K(z,t) = 2k\sqrt{\nu}e^{-ift}\frac{e^{-z^2/(4\nu t)}}{\sqrt{\pi t}} - ife^{(4k^2\nu-if)t}\sum_{\pm}\frac{e^{\pm 2kz}}{2}\mathrm{erfc}\left(\sqrt{4k^2\nu t}\pm\frac{z}{\sqrt{4\nu t}}\right), \tag{10}$$

where $\sum_{\pm}$ denotes the sum of the plus and minus terms and the complementary error function $\mathrm{erfc}(x) = 1-\mathrm{erf}(x)$. An equivalent form emphasizing dependence on wave parameters uses the scaled error function $\mathrm{erfcx}(t) = e^{t^2}\mathrm{erfc}(t)$ and reads

$$K(z,t) = 2k\sqrt{\nu}e^{-ift}\frac{e^{-z^2/(4\nu t)}}{\sqrt{\pi t}} - ife^{-ift}\frac{e^{-z^2/(4\nu t)}}{2}\sum_{\pm}\mathrm{erfcx}\left(\sqrt{4k^2\nu t}\pm\frac{z}{\sqrt{4\nu t}}\right). \tag{11}$$

Table 1
Asymptotic Behavior of the Ekman-Stokes Kernel K(z, t)

Limit	Behavior	Theory
$t \to \infty$	$2k\sqrt{\nu}e^{-ift}/\sqrt{\pi t}\left[1 - if/(4k^2\nu)\left(1 - (1 + 2k^2z^2)/(4k^2\nu t)\right)\right]$	long-time limit
$t \to 0^+$	$8\nu k^2\delta(z/\delta_S) - ife^{2kz}$	short-time limit
$\nu \to 0^+$	$-ife^{-ift}e^{2kz}$	Hasselmann (1970)
$f \to 0^+$	$2k\sqrt{\nu}e^{-z^2/(4\nu t)}/\sqrt{\pi t}$	Longuet-Higgins (1953)

The Ekman-Stokes kernel K captures the (Eulerian-mean) flow response to the Stokes drift. The $1/\sqrt{t}$ describes the establishment of an Ekman spiral driven by the wave stress; the if terms describe the impact of the Coriolis-Stokes forcing. Note that the dimension of $K(z, t)$ is time^{-1}.

Several limits of the kernel are of interest; they are given in dimensional terms in Table 1.

The limits $\nu \to 0^+$ and $f \to 0^+$ are best understood by rewriting (11) in terms of the dimensionless parameters $D = \delta_E/\delta_S$, $\zeta = 2kz$ and $\tau = ft$ to obtain

$$K(\zeta, \tau)/f = De^{-i\tau}\frac{e^{-\zeta^2/(2D^2\tau)}}{\sqrt{2\pi\tau}} - \frac{i}{2}\sum_{\pm} e^{-i\tau-\zeta^2/(2D^2\tau)}\mathrm{erfcx}\left(D\sqrt{\frac{\tau}{2}} \pm \frac{\zeta}{\sqrt{2D^2\tau}}\right). \quad (12)$$

When $D \gg 1$, for example, because $f \to 0^+$, the Coriolis-Stokes sum term in (12) is negligible and the flow becomes the Longuet-Higgins (1953) response to the wave stress at the surface. In contrast, for $D \ll 1$, for example, as $\nu \to 0^+$, the anti-Stokes result of Hasselmann (1970) is approached nonuniformly in ζ. This singular behavior arises since for any $D \neq 0$ the shear condition at the surface cannot be met by an exact anti-Stokes flow, so in a thin layer of depth $\sim\sqrt{\nu/f}$ near the surface cancelation of the Stokes drift is imperfect (e.g., Seshasayanan & Gallet, 2019). Over long times $\tau \to \infty$, the Coriolis-Stokes terms decay on the viscous rather than the inertial timescale, despite being caused by Earth's rotation.

The magnitude and argument of the dimensionless kernel $K(\zeta, \tau)$ are shown in Figure 1 for $D = 1$. The magnitude is largest toward $(\tau, \zeta) = (0, 0)$ due to the singular behavior discussed above. The kernel has the character of an amplitude-decaying inertial oscillation with period $2\pi/f$ with an orientation in the horizontal plane that oscillates with the inertial period.

Equation 11 together with the convolution in time (8) is the key result of this letter. Taking as inputs a time series of Stokes drift and estimates of the peak wave number k, Coriolis parameter f, and turbulent

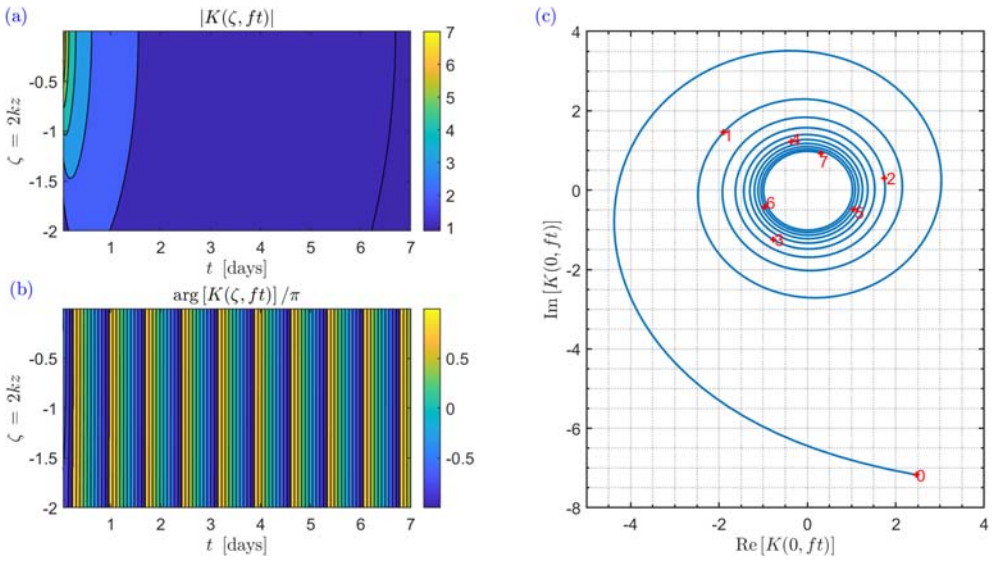

Figure 1. Ekman-Stokes kernel $K(\zeta, \tau)$ for $D = 1$ (with $f = 1 \times 10^{-4}\mathrm{s}^{-1}$): (a) magnitude and (b) argument as a function of depth and time and (c) hodograph at the surface ($\zeta = 0$) with time (in days) shown in red. In panel (a) we have saturated the color scale, as the kernel is singular at $(\zeta, \tau) = (0, 0)$.

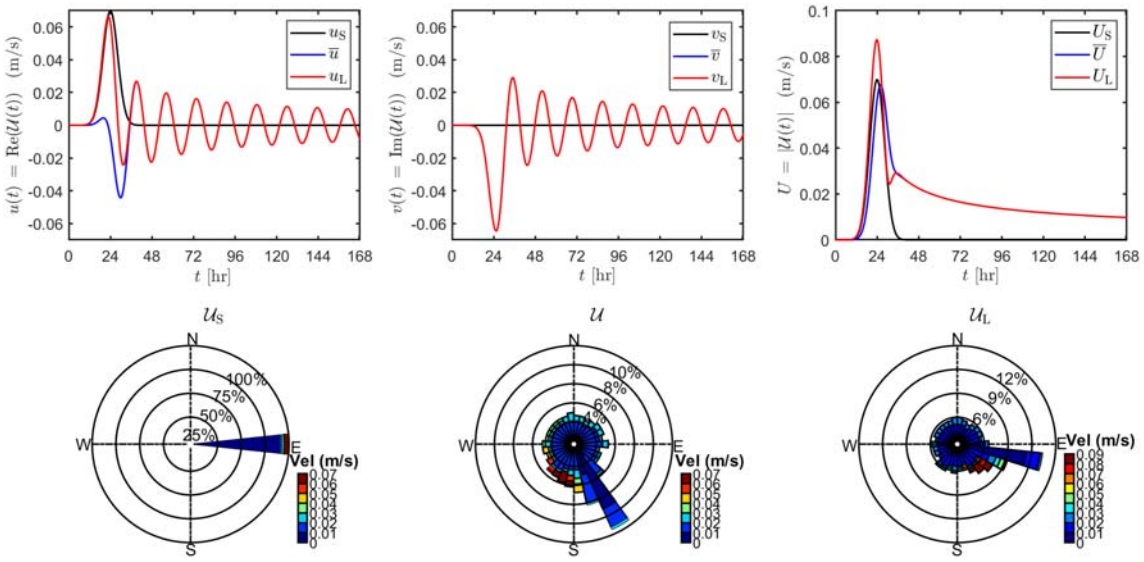

Figure 2. Top: time series of wave-induced velocities formed in response to an idealized 24 hr Gaussian storm in the Northern Hemisphere showing the two components and magnitude of the Stokes drift $\mathcal{U}_S$ (black), Eulerian-mean velocity $\mathcal{U}$ (blue) and Lagrangian velocity $\mathcal{U}_L$ (red). Bottom: wave roses for $\mathcal{U}_S, \mathcal{U}$, and $\mathcal{U}_L$, with radial distance representing the fraction of time during which the velocity has a given direction, and color indicating magnitude in m/s.

viscosity ν, these equations produce a time series of the associated (Eulerian-mean) Ekman-Stokes current at any vertical elevation z, which can simply be added to the Stokes drift time series to give the Lagrangian-mean current relevant for marine litter transport. An open-source implementation in Python is provided as supporting information.

3. Sample Calculations of the Ekman-Stokes Flow

3.1. Idealized Storm

To demonstrate the use of the Ekman-Stokes kernel, we calculate the Eulerian response to an idealized Gaussian storm lasting approximately 24 hr. Specifically, we set $u_S(z=0) = u_S^* \exp(-(t-t^*)^2/(\sigma^2))$ (and $v_S = 0$) with $\sigma = 6$ hr and magnitude $u_S^* = 0.070$ m/s being reached at $t^* = 24$ hr. Choosing $f = 1.0\times10^{-4}$ s^{-1} and $\nu = 1.0\times10^{-2}$ m^2 s^{-1} ($D = 1.1$), we set $\mathcal{U}(z=0, t=0) = 0$ and evaluate the response for 1 week.

In Figure 2 we plot the u and v components and magnitudes, respectively, of the second-order currents over a week-long period. The sum of Stokes drift (black) and Ekman-Stokes flow (blue) gives the Lagrangian velocity (red). Beneath, wave roses are plotted for these second-order currents. The angular direction corresponds to the angle of propagation of the flow (separated into 30 bins), the radius of each bar represents the percentage of time during which the velocity has a given direction, and the color scale divides the data into velocity amplitude ranges. Figure 2 shows that the Stokes drift is reduced by a (delayed) partial "anti-Stokes" flow, a transverse component arises on the same time scale, and damped inertial oscillations are formed that remain after the storm has ceased. The resulting Lagrangian current is deflected by the large transverse component of the Ekman-Stokes flow, to the right in the Northern Hemisphere (and to the left in the Southern Hemisphere).

3.2. Buoy Data

We use half-hourly records for the San Nicolas Island buoy (33.22° N, 119.88° W) obtained from CDIP (the Coastal Data Information Project) and estimate the Stokes drift using the formula

$$\mathcal{U}_S = g^{-1}\omega_p^3 A_p^2 \exp(2\bar{k}z)\exp\left(i\theta_p\right), \text{ where } A_p = H_S/\left(2\sqrt{2}\right), \tag{13}$$

where θ_p is the peak wave direction, H_s the significant wave height, and ω_p the peak frequency calculated from the peak period T_p. By making a quasi-monochromatic approximation, we assume the wave number spectrum is peaked about $k = \mathrm{mean}(k_p) = \mathrm{mean}(\omega_p^2/g)$, to leading order. We integrate (11) using the Stokes drift (13) by a trapezoidal rule with time step equal to the buoy sampling time. Defining the surface value

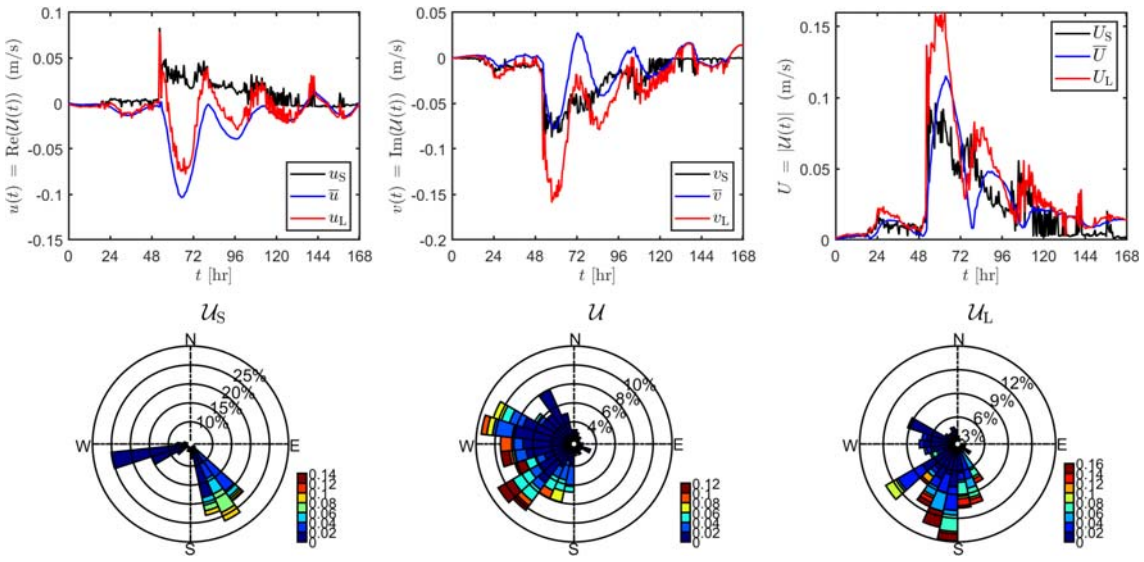

Figure 3. Top: time series (14 May 2000 15:41 to 22 May 2000 09:41 UTC) of wave-induced velocities computed from buoy data from San Nicolas Island (33.22° N, 119.88° W), with colors as in Figure 2. Bottom: corresponding wave roses, as in Figure 2.

of the kernel as $\lim_{z\to 0^-} K(z,t)$ instead of directly setting $z = 0$ allows the singular behavior at $(0,0)$ to be avoided.

As in Figure 2, the top panels of Figure 3 show u and v components and magnitudes of the second-order currents. The largest Stokes drift at San Nicolas Island over this time period is in a south-southeasterly direction, though a share of very small values arising from small-amplitude waves are also seen to propagate west-southwest (cf. bottom-left panel, Figure 3). In contrast, the Ekman-Stokes contribution is much more directionally spread at all velocity amplitudes due to excited inertial oscillations. Superimposing the two flows leads to a directionally spread Lagrangian drift, which veers to the right of the Stokes drift.

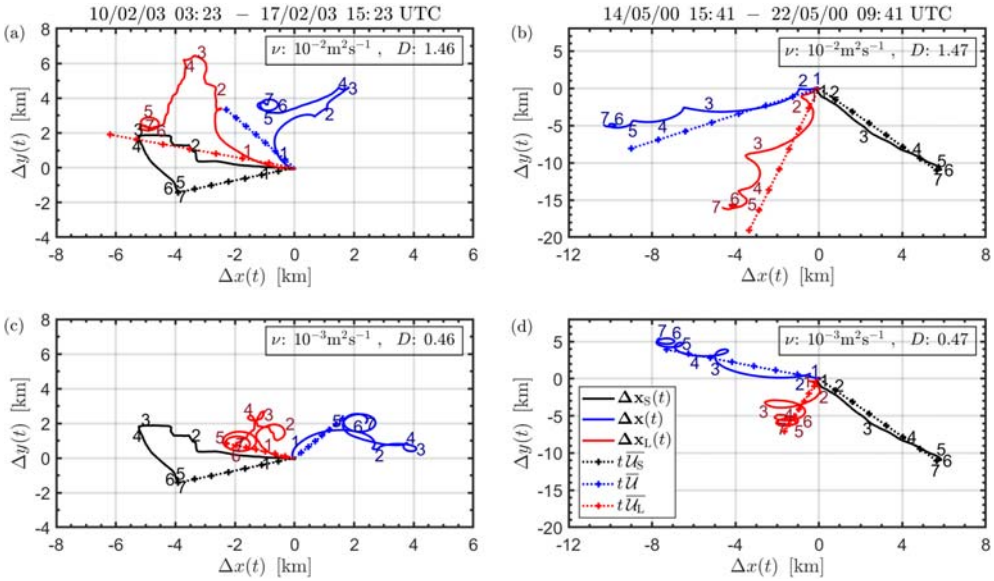

Figure 4. Particle paths at the surface ($z = 0$) computed for the San Nicolas Island buoy using our Ekman-Stokes convolution kernel. Columns: two different time samples. Rows: different values of turbulent viscosity. Paths shown are obtained using the Stokes drift (black), Eulerian-mean velocity, (blue) and Lagrangian-mean velocity (red). Dashed lines ignore time dependence of the Stokes drift and show the steady response to the average of the Stokes drift over the periods considered. All paths begin at $(\Delta x, \Delta y) = (0, 0)$. Numbers beside each line denote the number of days elapsed.

To find the displacement associated with the unsteady flows, we take the wave number and Stokes drift time series to be uniform in space, which is valid for the relatively small accumulated displacements considered. Particle displacements computed by time integrating the velocities obtained from our Ekman-Stokes kernel are plotted in Figure 4. Figures 4a and 4c show displacements over 1 week in February 2003 and Figures 4b and 4d over a week in May 2000, with (*b*) corresponding to velocities plotted in Figure 3. Line colors are consistent with Figures 2 and 3. Straight dotted lines represent steady solutions, that is, (7) multiplied by time elapsed, with $\overline{\mathcal{U}_S} = \text{mean}\left(\mathcal{U}_S\right)$. Evidently, the steady approximation causes errors in the prediction of net particle displacement. Instead of following the black trajectory described by the Stokes drift alone, we predict the particle will follow the red trajectory, being transported by the Lagrangian velocity, the sum of the Stokes drift, and wave-induced Ekman-Stokes flow. For both time samples, the Lagrangian displacement is to the right of the Stokes displacement, as for the velocities (in the Southern Hemisphere, it will lie to the left).

We anticipate that the realistic range for eddy viscosity is $O(10^{-3})$–$O(10^{-2})\,\mathrm{m^2\,s^{-1}}$, estimated from the vertical mixing coefficient $S_M = 0.30$ in Mellor and Blumberg (2004) by using the law of the wall. Comparing (c) and (d) with (a) and (b), particle displacement is reduced and inertial oscillations more pronounced for the smaller viscosity $\nu = 10^{-3}\mathrm{m^2\,s^{-1}}$ in (*c*) and (*d*), since the anti-Stokes flow increases in magnitude as viscosity decreases. For the realistic range of ν the displacement is significantly altered in both magnitude and direction when the Ekman-Stokes flow is included.

4. Discussion and Conclusions

Our analysis has demonstrated the need to add a so-called Ekman-Stokes flow to the Stokes drift to properly estimate the wave-induced Lagrangian-mean flow, which transports floating marine litter. We have derived an Ekman-Stokes convolution kernel, which can readily be used to predict the wave-induced Eulerian-mean flow in the turbulent upper-ocean boundary layer. It integrates three important effects: the surface wave stress, the Coriolis-Stokes forcing, and unsteadiness of the forcing and response.

We properly account for the viscous wave stress at the surface. This is often neglected (e.g., Lewis & Belcher, 2004; Onink et al., 2019; Polton et al., 2005), though it may be of similar magnitude to the wind stress. Including the wave stress should yield more accurate predictions of the Lagrangian drift, particularly when wind and waves are misaligned. Our model also incorporates the Coriolis-Stokes forcing, which induces a partial anti-Stokes flow and alters the response over the Ekman depth $\delta_E = \sqrt{2\nu/f}$ (cf. Polton et al., 2005). Our results demonstrate that for realistic eddy viscosities 10^{-3}–$10^{-2}\,\mathrm{m^2\,s^{-1}}$, the Stokes drift is only partially canceled by an anti-Stokes flow. Perhaps most importantly, our approach shows that unsteadiness of the Stokes drift and induced Eulerian response can be readily incorporated into models of Lagrangian drift using a simple convolution. As passage times of storms are typically $O(1/f)$, accounting for time variability is crucial for accurate predictions of drift.

Future work should improve our model in the following four ways. First, for simplicity we have assumed a constant eddy viscosity, although our kernel approach could be adapted for linearly increasing eddy viscosity (Lewis & Belcher, 2004; Madsen, 1977), which provides a more accurate representation of turbulence in the upper-ocean boundary layer. Second, Shrira and Almelah (2020) have presented a solution method incorporating time dependence of the eddy viscosity due to processes such as mixed-layer restratification or wave breaking (Price & Sundermeyer, 1999). Parameterizations of turbulent viscosity should thus account for both time and depth variation.

Third, while we have used a quasi-monochromatic assumption in our model, the Ekman-Stokes kernel can in principle be applied to broadbanded spectra using an additional integration over frequency. For typical broadbanded spectra, the near-surface Stokes drift is more strongly sheared than for a monochromatic wave corresponding to the peak frequency (Webb & Fox-Kemper, 2011). Therefore, the wave stress dominates the forcing of the Eulerian-mean flow whose magnitude is strengthened and whose direction becomes more aligned with that of the Stokes drift, as we have confirmed in preliminary computations. We emphasize that the wave stress is proportional to the fifth moment of the frequency spectrum and hence ill-defined for most empirical spectra, whose high-frequency tails behave like ω^{-4} or ω^{-5} (Breivik et al., 2016). This indicates a high sensitivity of the wave-induced mean flow to the spectral tail, suggesting the need for a careful assessment of the form of this tail and of its impact on the Eulerian-mean dynamics. We note that Seshasayanan and Gallet (2019) recently showed that the steady Ekman-Stokes current is unstable to perturbations. Future

work should consider the importance of this instability in the real ocean and how it might interact with unsteadiness of the wave-induced flow.

Fourth, ocean transport can be modeled using the tracer equation rather than Lagrangian tracking methods (Dobler et al., 2019; Wu et al., 2019). Stokes advection plays an important role in strong wind/wave conditions and affects up-/down-welling in coastal regions (Suzuki & Fox-Kemper, 2016; Wu et al., 2019). We anticipate that including the unsteady Ekman-Stokes flow will cause variations in up-/down-welling velocities over timescales $\gtrsim O(1/f)$ (section 4; Hasselmann, 1970; McWilliams & Restrepo, 1999).

Data Availability Statement

Buoy data were obtained from the Coastal Data Information Program (CDIP) (https://cdip.ucsd.edu). Data corresponding to the time series used in this paper are available in the supporting information.

Acknowledgments
T. S. v. d. B. was supported by a Royal Academy of Engineering Research Fellowship and J. V. by the UK Natural Environment Research Council Grant NE/R006652/1. The authors thank Harry Cunningham for assistance writing the Python script in the supporting information. The authors are grateful to Ø. Breivik for advice on how to obtain representative values of viscosity. The authors thank two referees whose comments have improved this paper and enriched the discussion of future work in section 4.

References

Andrady, A. L. (2011). Microplastics in the marine environment. *Marine Pollution Bulletin*, *62*(8), 1596–1605. https://doi.org/10.1016/j.marpolbul.2011.05.030

Bühler, O. (2014). *Waves and mean flows* (2nd ed.). Cambridge, UK: Cambridge University Press.

Breivik, Ø., Bidlot, J. R., & Janssen, P. (2016). A stokes drift approximation based on the phillips spectrum. *Ocean Modelling*, *100*, 49–56. https://doi.org/10.1016/j.ocemod.2016.01.005

Breivik, Ø., Janssen, P., & Bidlot, J-R. (2014). Approximate Stokes drift profiles in deep water. *Journal of Physical Oceanography*, *44*(9), 2433–2445. https://doi.org/10.1175/JPO-D-14-0020.1

Breivik, Ø., Mogensen, K., Bidlot, J-R., Balmaseda, M. A., & Janssen, P. (2015). Surface wave effects in the NEMO ocean model: Forced and coupled experiments. *Journal of Geophysical Research: Oceans*, *120*, 2973–2992. https://doi.org/10.1002/2014JC010565

Cózar, A., Echevarría, F., González-Gordillo, J. I., Irigoien, X., Úbeda, M., Hernández-León, S., et al. (2014). Plastic debris in the open ocean. *Science*, *111*(28), 10,239–10,244. https://doi.org/10.1073/pnas.1314705111

Delandmeter, P., & van Sebille, E. (2019). The parcels v2.0 Lagrangian framework: New field interpolation schemes. *Geoscientific Model Development*, *12*(8), 3571–3584. https://doi.org/10.5194/gmd-12-3571-2019

Dobler, D., Huck, T., Maes, C., Grima, N., Blanke, B., Martinez, E., & Ardhuin, F. (2019). Large impact of Stokes drift on the fate of surface floating debris in the South Indian Basin. *Marine Pollution Bulletin*, *148*, 202–209. https://doi.org/10.1016/j.marpolbul.2019.07.057

Ekman, V. W. (1905). On the influence of the Earth's rotation on ocean-currents. *Arkiv För Matematik, Astronomi Och Fysik*, *2*(11), 1–53.

Eriksen, M., Lebreton, L. C. M., Carson, H. S., Thiel, M., Moore, C. J., Borerro, J. C., et al. (2014). Plastic pollution in the world's oceans: More than 5 trillion plastic pieces weighing over 250,000 tons afloat at sea. *PLoS ONE*, *9*(12), e111913. https://doi.org/10.1371/journal.pone.0111913

Fraser, C., Morrison, A., Hogg, A. McC., Macaya, E., van Sebille, E., Ryan, P., et al. (2018). Antarctica's ecological isolation will be broken by storm-driven dispersal and warming. *Nature Climate Change*, *8*(8). https://doi.org/10.1038/s41558-018-0209-7

Geyer, R., Jambeck, J. R., & Lavender Law, K. (2017). Production, use, and fate of all plastics ever made. *Science Advances*, *3*(7), e1700782. https://doi.org/10.1126/sciadv.1700782

Goldstein, M. C., Rosenberg, M., & Cheng, L. (2012). Increased oceanic microplastic debris enhances oviposition in an endemic pelagic insect. *Biology Letters*, *8*, 817–20. https://doi.org/10.1098/rsbl.2012.0298

Grue, J., & Kolaas, J. (2017). Experimental particle paths and drift velocity in steep waves at finite water depth. *Journal of Fluid Mechanics*, *810*, R1. https://doi.org/10.1017/jfm.2016.726

Hasselmann, K. (1970). Wave-driven inertial oscillations. *Geophysical Fluid Dynamics*, *1*, 463–502. https://doi.org/10.1080/03091927009365783

Huang, N. E. (1979). On surface drift currents in the ocean. *Journal of Fluid Mechanics*, *91*(1), 191–208. https://doi.org/10.1017/S0022112079000112

Iwasaki, S., Isobe, A., Kako, S., Uchida, K., & Tokai, T. (2017). Fate of microplastics and mesoplastics carried by surface currents and wind waves: A numerical model approach in the Sea of Japan. *Marine Pollution Bulletin*, *121*(1), 85–96. https://doi.org/10.1016/j.marpolbul.2017.05.057

Jambeck, J. R., Geyer, R., Wilcox, C., Siegler, T. R., Perryman, M., Andrady, A., et al. (2015). Plastic waste inputs from land into the ocean. *Science*, *347*(6223), 768–771. https://doi.org/10.1126/science.1260352

Lavender Law, K. (2017). Plastics in the marine environment. *Annual Review of Marine Science*, *9*, 205–229. https://doi.org/10.1146/annurev-marine-010816-060409

Lebreton, L., Egger, M., & Slat, B. (2019). A global mass budget for positively buoyant macroplastic debris in the ocean. *Scientific Reports*, *9*, 12922. https://doi.org/10.1038/s41598-019-49413-5

Lewis, D. M., & Belcher, S. E. (2004). Time-dependent, coupled, Ekman boundary layer solutions incorporating Stokes drift. *Dynamics of Atmospheres and Oceans*, *37*(4), 313–351. https://doi.org/10.1016/j.dynatmoce.2003.11.001

Longuet-Higgins, M. S. (1953). Mass transport in water waves. *Philosophical Transactions of the Royal Society A*, *245*(903), 535–581. https://doi.org/10.1098/rsta.1953.0006

Madsen, O. S. (1977). A realistic model of the wind-induced Ekman boundary layer. *Journal of Physical Oceanography*, *7*(2), 248–255. https://doi.org/10.1175/1520-0485(1977)007<0248:ARMOTW>2.0.CO;2

Madsen, O. S. (1978). Mass transport in deep-water waves. *Journal of Physical Oceanography*, *8*(6), 1009–1015. https://doi.org/10.1175/1520-0485(1978)008<1009:MTIDWW>2.0.CO;2

McWilliams, J. C., & Fox-Kemper, B. (2013). Oceanic wave-balanced surface fronts and filaments. *Journal of Fluid Mechanics*, *730*, 464–490. https://doi.org/10.1017/jfm.2013.348

McWilliams, J. C., & Restrepo, J. M. (1999). The wave-driven ocean circulation. *Journal of Physical Oceanography*, *29*(10), 2523–2540. https://doi.org/10.1175/1520-0485(1999)029<2523:TWDOC>2.0.CO;2

Mellor, G., & Blumberg, A. (2004). Wave breaking and ocean surface layer thermal response. *Journal of Physical Oceanography*, *34*(3), 693–698. https://doi.org/10.1175/2517.1

Onink, V., Wichmann, D., Delandmeter, P., & van Sebille, E. (2019). The role of Ekman currents, geostrophy, and Stokes drift in the accumulation of floating microplastic. *Journal of Geophysical Research: Oceans*, *124*, 1474–1490. https://doi.org/10.1029/2018JC014547

Ostle, C., Thompson, R. C., Broughton, D., Gregory, L., Wootton, M., & Johns, D. G. (2019). The rise in ocean plastics evidenced from a 60-year time series. *Nature Communications*, *10*, 1622. https://doi.org/10.1038/s41467-019-09506-1

Polton, J. A., Lewis, D. M., & Belcher, S. E. (2005). The role of wave-induced Coriolis-Stokes forcing on the wind-driven mixed layer. *Journal of Physical Oceanography*, *35*(4), 444–457. https://doi.org/10.1175/JPO2701.1

Price, J. F., & Sundermeyer, M. A. (1999). Stratified Ekman layers. *Journal of Geophysical Research*, *104*(C9), 20,467–20,494. https://doi.org/10.1029/1999JC900164

Seshasayanan, K., & Gallet, B. (2019). Surface gravity waves propagating in a rotating frame: The Ekman-Stokes instability. *Physical Review Fluids*, *4*, 104802.

Shrira, V. I., & Almelah, R. B. (2020). Upper-ocean Ekman current dynamics: A new perspective. *Journal of Fluid Mechanics*, *887*, A24. https://doi.org/10.1017/jfm.2019.1059

Stokes, G. G. (1847). On the theory of oscillatory waves. *Transactions of the Cambridge Philosophical Society*, *8*, 441–455.

Suzuki, N., & Fox-Kemper, B. (2016). Understanding Stokes forces in the wave-averaged equations. *Journal of Geophysical Research: Oceans*, *121*, 3579–3596. https://doi.org/10.1002/2015JC011566

The WAMDI Group (1988). The WAM model—A third generation ocean wave prediction model. *Journal of Physical Oceanography*, *18*(12), 1775–1810. https://doi.org/10.1175/1520-0485(1988)018<1775:TWMTGO>2.0.CO;2

Tolman, H. L. (2009). User manual and system documentation of WAVEWATCH III TM version 3.14 Technical Note.

Ünlüata, Ü., & Mei, C. C. (1970). Mass transport in water waves. *Journal of Geophysical Research*, *75*(36), 7611–7618. https://doi.org/10.1029/JC075i036p07611

Ursell, F. (1950). On the theoretical form of ocean swell on a rotating earth. *Monthly Notices of the Royal Astronomical Society, Geophysical Supplement*, *6*(s1), 1–8. https://doi.org/10.1111/j.1365-246X.1950.tb02968.x

van Sebille, E., Aliani, S., Law, K. L., Maximenko, N., Alsina, J., Bagaev, A., et al. (2020). The physical oceanography of the transport of floating marine debris. *Environmental Research Letters*, *15*(2), 23003. https://doi.org/10.1088/1748-9326/ab6d7d

van Sebille, E., Wilcox, C., Lebreton, L., Maximenko, N., Hardesty, B. D., van Franeker, J. A., et al. (2015). A global inventory of small floating plastic debris. *Environmental Research Letter*, *10*(12), 124006. https://doi.org/10.1088/1748-9326/10/12/124006

van den Bremer, T. S., & Breivik, Ø. (2017). Stokes drift. *Philosophical Transactions of the Royal Society London A*, *376*, 2111. https://doi.org/10.1098/rsta.2017.0104

Webb, A., & Fox-Kemper, B. (2011). Wave spectral moments and Stokes drift estimation. *Ocean Modelling*, *40*(3), 273–288. https://doi.org/10.1016/j.ocemod.2011.08.007

Wilcox, C., Hardesty, B. D., & Law, K. L. (2020). Abundance of floating plastic particles is increasing in the western North Atlantic Ocean. *Environmental Science & Technology*, *54*(2), 790–796. https://doi.org/10.1021/acs.est.9b04812

Wu, L., Staneva, J., Breivik, Ø., Rutgersson, A., George Nurser, A. J., Clementi, E., & Madec, G. (2019). Wave effects on coastal upwelling and water level. *Ocean Modelling*, *140*, 101405. https://doi.org/10.1016/j.ocemod.2019.101405

Xu, Z., & Bowen, A. J. (1994). Wave- and wind-driven flow in water of finite depth. *Journal of Physical Oceanography*, *24*(9), 1850–1866. https://doi.org/10.1175/1520-0485(1994)024<1850:WAWDFI>2.0.CO;2